Economic Model Predictive Control of Transport-Reaction Processes

Liangfeng Lao,[†] Matthew Ellis,[†] and Panagiotis D. Christofides*,[†,‡]

[†]Department of Chemical and Biomolecular Engineering, University of California, Los Angeles, California 90095, United States
[‡]Department of Electrical Engineering, University of California, Los Angeles, California 90095, United States

ABSTRACT: This work focuses on the development of economic model predictive control (EMPC) systems for transport-reaction processes described by nonlinear parabolic partial differential equations (PDEs) and their applications to a non-isothermal tubular reactor where a second-order chemical reaction takes place. The tubular reactor is modeled by two nonlinear parabolic PDEs. Galerkin's method is used to derive finite-dimensional systems that capture the dominant dynamics of the parabolic PDEs which are subsequently used for the EMPC design. The EMPC formulation uses the integral of the reaction rate along the length of the reactor as an economic cost function subject to constraints on the control action and states over an operation period. Closed-loop simulations are conducted of a low-order EMPC system, formulated with a constraint on the available reactant material over each operation period, applied to a high-order discretization of the PDEs and of a high-order EMPC system formulated with a specific state constraint and with the constraint on the available reactant material. Simulation results demonstrate that the EMPC operates the process in a time-varying fashion and improves the economic cost over steady-state operation using the same amount of reactant material over a fixed period of operation, as well as meeting state constraints.

■ INTRODUCTION

Transport-reaction processes are characterized by significant spatial variations and nonlinearities due to the underlying diffusion and convection phenomena and complex reaction mechanisms, respectively. Currently, the approach followed for the solution of the control problem of transport-reaction processes is essentially determined by the well-known classification of PDE systems into hyperbolic, parabolic, or elliptic.[1] Specifically, processes whose convective mechanisms dominate over diffusive ones can be adequately described by systems of quasi-linear hyperbolic PDEs. However, the diffusive phenomena also play a prominent role in the dynamic models of several industrially important transport-reaction processes, e.g., tubular, fluidized bed, and packed bed reactors, and should be accounted for. These processes are typically modeled by quasi-linear parabolic PDEs whose spatial differential operators can be characterized by a spectrum that can be partitioned into a finite (possibly unstable) slow part and an infinite dimensional stable fast complement.[2]

On the basis of the above, the traditional approach to the control of quasi-linear parabolic PDEs involves the application of eigenfunction expansion techniques to the PDE system to derive systems of finite-dimensional ordinary differential equations (ODEs) that accurately describe the dynamics of the dominant (slow) modes of the PDE system. In detail, the solution of the original PDE system is initially expanded as the sum of an infinite series of the eigenfunctions of the spatial differential operator with time-varying coefficients. This expansion is used to derive an infinite set of ODEs for the coefficients of the expansion. Then, a finite-dimensional ODE model is derived by discarding an infinite set of equations. The finite-dimensional ODE model is subsequently used as the basis for the synthesis of finite-dimensional controllers (e.g., refs 3–5). A potential drawback of this approach is that the number of modes that should be retained to derive an ODE system which yields the desired degree of approximation may be very large. To overcome these

controller synthesis and implementation problems, research efforts focused on taking advantage of the concept of inertial manifold (IM) (e.g., ref 6) and approximate inertial manifolds (AIMs) (e.g., refs 7–9) for the construction of low-order ODE systems of desired accuracy. On the basis of this, significant work over the last 20 years has focused on the synthesis of low-order controllers for quasi-linear parabolic PDE systems on the basis of low-order nonlinear ODE models derived through a combination of Galerkin's method (using analytical or empirical basis functions) with the concept of approximate inertial manifolds (e.g., refs 9–11 and the book[12] for results and references in this area).

Model predictive control (MPC), known also as receding horizon control, is a popular control method for handling constraints (both on manipulated inputs and state variables) within an optimal control setting. Numerous research studies have investigated the properties of model predictive controllers and led to a plethora of MPC formulations that focus on a number of control-relevant issues, including issues of closed-loop stability, performance, implementation, and constraint satisfaction (e.g., refs 13–15 for results and references in this area). In the past 10 years, significant work has been done on the application of MPC to distributed parameter systems. Contributions include analyzing the predictive control problem on the basis of the infinite-dimensional system using control Lyapunov functionals,[16] the use of the finite difference method to derive approximate ODE models for MPC design,[17] the methodology of model predictive control design for highly dissipative PDEs,[18] and the application of MPC to a catalytic

reverse flow reactor (RFR).[19] Furthermore, computationally efficient predictive control algorithms for nonlinear parabolic and hyperbolic PDEs with state and control constraints have been proposed in refs 20−22.

Economic MPC (EMPC) has been extensively studied recently in the context of finite dimensional systems (e.g., refs 23−27 for results and references in this area). The work of ref 24 deals with a reformulation of the conventional MPC quadratic cost function in which an economic (not necessarily quadratic) cost function is used directly as the cost in MPC, and thus, it may, in general, lead to time-varying process operation policies (instead of steady-state operation), which directly optimize process economics. Most of the research in the area of EMPC, however, has focused on lumped-parameter processes modeled by ODE systems. Compared with lumped-parameter systems, no work has been done on the problem of designing EMPC for distributed parameter systems modeled by PDEs. Moreover, operation of transport-reaction processes typically requires that the state of the closed-loop system be maintained within certain bounds to achieve acceptable performance like requiring the temperature of a tubular reactor not to exceed a certain limit, and is also limited by the finite capacity of control actuators and constraints on reactant availability. Therefore, EMPC of parabolic PDEs is an important theoretical problem with practical implications.

In this work, we focus on the development of economic model predictive control (EMPC) systems for transport-reaction processes that are described by nonlinear parabolic partial differential equations (PDEs). Through the application of Galerkin's method, finite-dimensional ordinary differential equation models are first derived that capture the dominant dynamics of the parabolic PDEs. The reduced-order models are then used to formulate finite-dimensional EMPC systems of varying dimension depending on the type of state constraints imposed. The EMPC systems are applied to a non-isothermal tubular reactor, described by two nonlinear parabolic PDEs, where a second-order chemical reaction takes place. A state constraint that bounds the reactor temperature as well as an input constraint that bounds the available reactant material over a fixed period of operation are considered in the formulations of the EMPC systems which use the average reaction rate along the length of the reactor as the economic cost function. Closed-loop simulations are conducted where a low-order EMPC system and a high-order EMPC system are separately applied to a high-order discretization of the reactor PDE model, and they demonstrate that the EMPC systems operate the process in a time-varying fashion to improve the economic cost over steady-state operation and meet input and state constraints.

■ PRELIMINARIES

Class of Parabolic PDE Systems. In this work, we consider parabolic partial differential equation systems with a state-space representation of the following form:

$$\frac{\partial \overline{x}}{\partial t} = A\frac{\partial \overline{x}}{\partial z} + B\frac{\partial^2 \overline{x}}{\partial z^2} + Wu(t) + f(\overline{x}(z, t)) \tag{1}$$

subject to the boundary conditions:

$$\frac{\partial \overline{x}}{\partial z} = g_0\overline{x}, \quad z = 0$$

$$\frac{\partial \overline{x}}{\partial z} = g_1\overline{x}, \quad z = 1 \tag{2}$$

and the initial condition:

$$\overline{x}(z, 0) = \overline{x}_0(z) \tag{3}$$

where $\overline{x}(z, t) = [\overline{x}_1(z, t) \dots \overline{x}_{n_x}(z, t)]'$ denotes the state vector of the system, the notation $\overline{x}'$ denotes the transpose of $\overline{x}$, $f(\overline{x}(z, t))$ denotes a nonlinear vector function, $z \in [0, 1]$ is the spatial coordinate, $t \in [0, \infty)$ is the time, A, B, W, g_0, and g_1 are matrices and vectors of appropriate dimensions, and $u(t)$ denotes the n_u-dimensional manipulated input vector and is subject to the following input constraints:

$$u_{min} \leq u(t) \leq u_{max} \tag{4}$$

where u_{min} and u_{max} are the lower and upper bound vectors of the manipulated input $u(t)$. Moreover, the system states are also subject to the following constraints:

$$x_{min} \leq \int_0^1 r_x(z)\overline{x}(z, t) \, dz \leq x_{max} \tag{5}$$

where x_{min} and x_{max} are the lower and upper state constraints, respectively. The function $r_x(z) \in L_2(0,1)$ is the state constraint distribution function used to describe how the state constraint is enforced in the spatial domain $[0, 1]$, and $L_2(0, 1)$ is used to denote the space of measurable functions that are square-integrable on the interval $[0, 1]$.

Galerkin's Method. To present our results, we first formulate the PDE system as an infinite dimensional system in the Hilbert space $\mathcal{H}([0, 1]; \text{IR}^{n_x})$, with $\mathcal{H}$ being the space of measurable vector functions defined on $[0, 1]$, with inner product and norm:

$$(\omega_1, \omega_2) = \int_0^1 (\omega_1(z), \omega_2(z))_{\text{IR}^{n_x}} \, dz,$$

$$\|\omega_1\|_2 = (\omega_1, \omega_1)^{1/2} \tag{6}$$

where ω_1 are ω_2 are two elements of $\mathcal{H}([0, 1]; \text{IR}^{n_x})$ and the notation $(\cdot, \cdot)_{\text{IR}^{n_x}}$ denotes the standard inner product in IR^{n_x}. The state function $x(t)$ on the state-space $\mathcal{H}$ is defined as

$$x(t) = \overline{x}(z, t), \quad t > 0, \quad 0 \leq z \leq 1 \tag{7}$$

and the operator $\mathcal{A}$ is defined as

$$\mathcal{A}x = A\frac{d\overline{x}}{dz} + B\frac{d^2\overline{x}}{dz^2}, \quad 0 \leq z \leq 1 \tag{8}$$

Then, the system of eq 1 takes the following infinite-dimensional quasi-linear form:

$$\dot{x}(t) = \mathcal{A}x(t) + \mathcal{B}u(t) + \mathcal{F}(x(t)), \quad x(0) = x_0 \tag{9}$$

where $x_0 = \overline{x}_0(z)$, $\mathcal{B}u(t) = Wu(t)$, and $\mathcal{F}(x(t))$ is a nonlinear vector function in the Hilbert space. For the operator $\mathcal{A}$, the eigenvalue problem takes the form

$$\mathcal{A}\phi_k = \lambda_k\phi_k, \quad k = 1, ..., \infty \tag{10}$$

subject to

$$\frac{d\phi_k}{dz}(0) = g_0\phi_k(0)$$

$$\frac{d\phi_k}{dz}(1) = g_1\phi_k(1) \tag{11}$$

where ϕ_k is an eigenfunction corresponding to the kth eigenvalue and $\overline{\phi}_k$ is an adjoint eigenfunction of the operator $\mathcal{A}$.

Assumption 1 below characterizes the class of parabolic PDEs considered in this work and states that the eigenspectrum of operator $\mathcal{A}$ can be partitioned into a finite part consisting of m slow eigenvalues which are close to the imaginary axis and a stable infinite complement containing the remaining fast eigenvalues which are far in the left half of the complex plane, and that the separation between the slow and fast eigenvalues of $\mathcal{A}$ is large. We also note that the large separation between slow and fast modes of the spatial operator in parabolic PDEs ensures that a controller which exponentially stabilizes the closed-loop ODE system also stabilizes the closed-loop infinite-dimensional system.[3] This assumption is satisfied by the majority of diffusion-convection-reaction processes.[12]

Assumption 1.

(1) $Re(\lambda_1) \geq Re(\lambda_2) \geq ... \geq Re(\lambda_j) \geq ...$, where $Re(\lambda_j)$ denotes the real part of the eigenvalue, λ_j.

(2) The eigenspectrum of $\mathcal{A}$, $\sigma(\mathcal{A})$, is defined as the set of all eigenvalues of $\mathcal{A}$, i.e., $\sigma(\mathcal{A}) = \{\lambda_1, \lambda_2, ...\}$. $\sigma(\mathcal{A})$ can be partitioned as $\sigma(\mathcal{A}) = \sigma_1(\mathcal{A}) \cup \sigma_2(\mathcal{A})$, where $\sigma_1(\mathcal{A})$ consists of the first m finite eigenvalues, i.e., $\sigma_1(\mathcal{A}) = \{\lambda_1, ..., \lambda_m\}$, and $|Re(\lambda_1)|/|Re(\lambda_m)| = O(1)$.

(3) $Re(\lambda_{m+1}) < 0$ and $|Re(\lambda_1)|/|Re(\lambda_{m+1})| = O(\varepsilon)$, where $\varepsilon < 1$ is a small positive number.

Next, we apply the standard Galerkin's method to the infinite-dimensional system of eq 9 to derive a finite-dimensional system. Let $\mathcal{H}_s$ and $\mathcal{H}_f$ be modal subspaces of $\mathcal{A}$ defined as $\mathcal{H}_s = \text{span}\{\phi_1, \phi_2, ..., \phi_m\}$ and $\mathcal{H}_f = \text{span}\{\phi_{m+1}, \phi_{m+2}, ...\}$. The existence of $\mathcal{H}_s$ and $\mathcal{H}_f$ follows from the properties of $\mathcal{A}$. Defining the orthogonal projection operators, P_s and P_f, which project the state x onto the subspaces $\mathcal{H}_s$ and $\mathcal{H}_f$ of $\mathcal{A}$, respectively (i.e., $x_s = P_s x \in \mathcal{H}_s$ and $x_f = P_f x \in \mathcal{H}_f$), the state x of the system of eq 9 can be decomposed as

$$x = x_s + x_f = P_s x + P_f x \tag{12}$$

Applying P_s and P_f to the system of eq 9 and using the above decomposition for x, the system of eq 9 can be rewritten in the following equivalent form:

$$\dot{x}_s(t) = \mathcal{A}_s x_s(t) + \mathcal{F}_s(x_s(t), x_f(t)) + \mathcal{B}_s u(t),$$
$$x_s(0) = P_s x(0) = P_s x_0,$$
$$\dot{x}_f(t) = \mathcal{A}_f x_f(t) + \mathcal{F}_f(x_s(t), x_f(t)) + \mathcal{B}_f u(t),$$
$$x_f(0) = P_f x(0) = P_f x_0 \tag{13}$$

where $\mathcal{A}_s = P_s\mathcal{A}$, $\mathcal{B}_s = P_s\mathcal{B}$, $\mathcal{A}_f = P_f\mathcal{A}$, $\mathcal{B}_f = P_f\mathcal{B}$, $\mathcal{F}_f = P_f\mathcal{F}$, and $\mathcal{F}_s = P_s\mathcal{F}$. In the above system, $\mathcal{A}_s = \text{diag}\{\lambda_j\}$, $j = 1, ..., m$, is a diagonal matrix of dimension $m \times m$ and may contain unstable eigenvalues (i.e., $Re(\lambda_j) > 0$). The operator $\mathcal{A}_f$ is an unbounded exponentially stable differential operator. Neglecting the fast modes, the resulting ODE system is

$$\dot{x}_s(t) = \mathcal{A}_s x_s(t) + \mathcal{F}_s(x_s(t), 0) + \mathcal{B}_s u(t), \quad x_s(0) = P_s x_0 \tag{14}$$

which is a finite-dimensional system that describes the slow (dominant) dynamics of the PDE system of eq 1 and may be used for standard model-based control synthesis.

Remark 1. Whenever the eigenfunction ϕ_j of the operator $\mathcal{A}$ cannot be calculated analytically, one can still use Galerkin's method to perform model reduction by using the empirical eigenfunctions of the PDE system as basis functions in $\mathcal{H}_s$ and

$\mathcal{H}_f$ (such empirical eigenfunctions can be extracted from detailed numerical simulations of the PDE system using the Karhunen−Loeve expansion; see ref 28).

ECONOMIC MODEL PREDICTIVE CONTROL PROBLEM FORMULATION

We consider the application of economic model predictive control (EMPC) to the infinite-dimensional system of eq 9 to optimize an economic measure. We assume that the EMPC receives state measurements continuously and synchronously at sampling periods denoted as $t_k = k\Delta$ with $k = 0, 1, ...$. The EMPC optimization problem has the form

$$\max_{u \in S(\Delta)} \int_{t_k}^{t_{k+N}} L(\tilde{x}(\tau), u(\tau)) \, d\tau \tag{15a}$$

$$\text{s.t.} \quad \dot{\tilde{x}}(t) = \mathcal{A}\tilde{x}(t) + \mathcal{F}(\tilde{x}(t)) + \mathcal{B}u(t) \tag{15b}$$

$$\tilde{x}(t_k) = x(t_k) \tag{15c}$$

$$u_{min} \leq u(t) \leq u_{max}, \, \forall \, t \in [t_k, t_{k+N}) \tag{15d}$$

$$x_{min} \leq (r_x, \tilde{x}(t)) \leq x_{max}, \, \forall \, t \in [t_k, t_{k+N}) \tag{15e}$$

where Δ is the sampling period, $S(\Delta)$ is the family of piecewise constant functions with sampling period Δ, N is the prediction horizon, $\tilde{x}(t)$ is the predicted state function evolution with input $u(t)$ computed by the EMPC, and $x(t_k)$ is the state measurements. In the optimization problem of eq 15, the cost function of eq 15a defined as $L(\tilde{x}(\tau), u(\tau))$ is formulated to directly account for the economics of the PDE system. The constraint of eq 15b is the PDE system in the Hilbert space used to predict the future evolution of the PDE system with the initial condition of eq 15c obtained through state feedback. The constraints of eqs 15d and e are the available control energy and state constraints, respectively. The optimal solution to this optimization problem is $u^*(t|t_k)$ defined for $t \in [t_k, t_{k+N})$. The EMPC applies the control action computed for the first sampling period to the system in a sample-and-hold fashion for $t \in [t_k, t_{k+1})$. The EMPC is resolved at the next sampling period, t_{k+1}, after receiving new state measurements, $x(t_{k+1})$. The infinite dimensional nature of the controller of eq 15 in this case, however, renders it unsuitable for the purpose of practical implementation.

Low-Order Economic Model Predictive Control Formulation. In this formulation, a Lyapunov-based EMPC (LEMPC) system (see ref 24 for results on LEMPC) is designed on the basis of the low-order, finite-dimensional slow subsystem of eq 14 describing the evolution of x_s (the fast subsystem is neglected). The low-order EMPC law is obtained by solving, in a receding horizon fashion, the following finite-dimensional optimization problem:

$$\max_{u \in S(\Delta)} \int_{t_k}^{t_{k+N}} L(\tilde{x}_s(\tau), u(\tau)) \, d\tau \tag{16a}$$

$$\text{s.t.} \quad \dot{\tilde{x}}_s(t) = \mathcal{A}_s \tilde{x}_s(t) + \mathcal{F}_s(\tilde{x}_s(t), 0) + \mathcal{B}_s u(t) \tag{16b}$$

$$\tilde{x}_s(t_k) = P_s x(t_k) \tag{16c}$$

$$u_{min} \leq u(t) \leq u_{max}, \, \forall \, t \in [t_k, t_{k+N}) \tag{16d}$$

$$x_{min} \leq (r_x, \tilde{x}_s(t)) \leq x_{max}, \, \forall \, t \in [t_k, t_{k+N}) \tag{16e}$$

$$(\tilde{x}_s(t), P\tilde{x}_s(t)) \leq \bar{\rho}, \, \forall \, t \in [t_k, t_{k+N}) \tag{16f}$$

The constraints of eqs 16b and c are used to predict the future evolution of the slow subsystem with the initial condition given

in eq 16c. The constraints of eqs 16d and e are the available control energy and the state constraints, respectively. The constraint of eq 16f is a quadratic Lyapunov function (P is an $m \times m$ dimensional positive definite matrix) of the slow subsystem and ensures that the predicted state trajectory is restricted inside a predefined stability region which is a level set of the Lyapunov function (see ref 24 for a complete discussion of this issue).

Remark 2. The reduced-order EMPC formulation may achieve suboptimal solutions compared to the infinite dimensional EMPC problem, but it is not possible to quantify how suboptimal the solution obtained via the reduced-order formulation is (due to the inability to compute the solution of the infinite-dimensional problem).

Remark 3. To improve the accuracy of the slow finite-dimensional x_s subsystem, the finite-dimensional approximation of the system of eq 14 may be obtained through combination of Galerkin's method with approximate inertial manifolds. This approach can be used to further reduce the dimension of the x_s subsystem and ensure that it is of an appropriately low order suitable for controller design and online controller implementation.[12]

High-Order Economic Model Predictive Control Formulation. Accounting for the evolution of the fast subsystem is important for the purpose of satisfying state constraints. To formulate a finite dimensional EMPC optimization problem, the fast subsystem is truncated at the lth fast state (i.e., the $l + 1, l + 2$, ... states are discarded). The notation $\hat{}$ is used to denote the finite-dimensional truncation of the fast subsystem. The computational complexity associated with accounting for the fast subsystem could be eased by neglecting the nonlinearity in the dynamic model of the fast modes, while retaining the nonlinear dynamics of the slow modes (so as to not adversely effect the task of stabilization). The term $\hat{\mathcal{A}}_f$ behaves like $1/\varepsilon$ (in Assumption 1), where ε is a small positive parameter. Therefore, $\hat{\mathcal{A}}_f$ is much greater than $\hat{\mathcal{F}}_f$ and $\hat{\mathcal{F}}_f$ can be neglected from the equation (see ref 12 for more discussion and analysis of this approximation). Using this approximation, the EMPC formulation takes the following form:

$$\max_{u \in S(\Delta)} \int_{t_k}^{t_{k+N}} L(\check{x}(\tau), u(\tau)) \, d\tau \tag{17a}$$

$$\text{s.t.} \quad \dot{\tilde{x}}_s(t) = \mathcal{A}_s \tilde{x}_s(t) + \mathcal{F}_s(\tilde{x}_s(t), \hat{x}_f(t)) \\ + \mathcal{B}_s u(t) \tag{17b}$$

$$\dot{\hat{x}}_f(t) = \hat{\mathcal{A}}_f \hat{x}_f(t) + \hat{\mathcal{B}}_f u(t) \tag{17c}$$

$$\tilde{x}_s(t_k) = P_s x(t_k), \quad \hat{x}(t_k) = \hat{P}_f x(t_k) \tag{17d}$$

$$\check{x}(t) = \tilde{x}_s(t) + \hat{x}_f(t) \tag{17e}$$

$$u_{\min} \leq u(t) \leq u_{\max}, \quad \forall \, t \in [t_k, t_{k+N}) \tag{17f}$$

$$x_{\min} \leq (r_x, \check{x}(t)) \leq x_{\max}, \quad \forall \, t \in [t_k, t_{k+N}) \tag{17g}$$

$$(\check{x}(t), P\check{x}(t)) \leq \bar{\rho} \tag{17h}$$

In the optimization problem of eq 17, the constraint of eq 17c is the finite-dimensional truncation of the fast subsystem (nonlinear part of the dynamics being neglected) which is used to predict the evolution of the fast subsystem states and $\check{x}(t)$ is used to denote the vector of all the states (i.e., both the slow subsystem and fast subsystem states). The cost function and the remaining constraints are similar to eq 16.

Remark 4. We choose a certain number of modes of the dynamic system of eqs 17b and 17c for the synthesis of the high-order EMPC formulation to make sure that further increase in the number of modes leads to identical numerical results.

Remark 5. State constraints arise either due to the necessity to keep the process state variables within acceptable ranges to avoid, for example, runaway reactions (in which case they need to be enforced at all times and treated as hard constraints) or due to the desire to maintain process state variables within desirable bounds dilated by performance considerations (in which case they may be relaxed, and treated as soft constraints). In the formulations presented in this work, we consider state constraints that are hard constraints but could also be treated as soft ones; for predictive controller formulations where the state constraints are handled as soft constraints, see, e.g., refs 29 and 30.

APPLICATION TO A TUBULAR REACTOR

In this section, we apply the low-order and high-order EMPC systems to a transport-reaction chemical process example. First, we present the model of the transport-reaction process which is a tubular reactor. Second, we apply Galerkin's method to the chemical process example to construct a reduced-order model in modal space. Finally, we present a series of simulations with EMPC systems formulated with various state and input constraints to assess the performance of the closed-loop system under the EMPC.

Reactor Description. We consider a non-isothermal tubular reactor shown in Figure 1, where an irreversible second-order
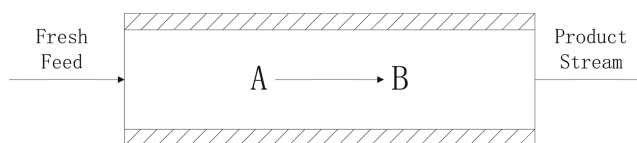

Figure 1. A tubular reactor with reaction A → B.

reaction of the form A → B takes place. The reaction is exothermic, and a cooling jacket of constant temperature is used to remove heat from the reactor. Under the standard assumptions of constant density (ρ) and heat capacity (C_p) of the reacting fluid, and constant axial fluid velocity (v), the dynamic model of the process can be derived from mass and energy balances and takes the following form:

$$\frac{\partial T}{\partial t} = -v \frac{\partial T}{\partial z} + \frac{k}{\rho C_p} \frac{\partial^2 T}{\partial z^2} + \left(\frac{-\Delta H k_0}{\rho C_p} \right) \exp\left(\frac{-E}{RT} \right) C_A^2 \\ - \frac{h A_s}{\rho C_p} (T - T_c)$$

$$\frac{\partial C_A}{\partial t} = -v \frac{\partial C_A}{\partial z} + D_A \frac{\partial^2 C_A}{\partial z^2} - k_0 \exp\left(\frac{-E}{RT} \right) C_A^2 \tag{18}$$

where T and C_A denote the temperature and concentration of species A in the reactor, respectively, k and D_A are the thermal conductivity and mass diffusivity of the reacting fluid, respectively, k_0, E, and $-\Delta H$ represent the pre-exponential constant, activation energy, and heat of the reaction, respectively, h is the heat transfer coefficient between the reactor and the cooling jacket, A_s is the surface area of the reactor walls, and T_c is the jacket temperature. The system is subject to the boundary conditions:

$$z = 0: \quad \frac{\partial T}{\partial z} = \frac{\rho C_p v}{k}(T - T_f), \quad \frac{\partial C_A}{\partial z} = \frac{v}{D_A}(C_A - C_{Af})$$

$$z = L: \quad \frac{\partial T}{\partial z} = 0, \quad \frac{\partial C_A}{\partial z} = 0$$

$$(19)$$

where T_f and C_{Af} denote the inlet temperature and concentration of species A in the reactor and L is the length of the reactor. In this case, we choose the inlet concentration of species A, C_{Af}, as the manipulated input. In order to simplify the presentation of our results, we introduce the following dimensionless variables:

$$\bar{t} = \frac{tv}{L}, \quad \bar{z} = \frac{z}{L}, \quad Pe_1 = \frac{\rho C_p v L}{k}, \quad Pe_2 = \frac{vL}{D_A},$$

$$\bar{x}_1 = \frac{T - T_0}{T_0}, \quad \bar{x}_2 = \frac{C_A - C_{A0}}{C_{A0}}, \quad u = \frac{C_{Af} - C_{A0}}{C_{A0}},$$

$$\gamma = \frac{E}{RT_0}, \quad T_s = \frac{T_c - T_0}{T_0}, \quad T_i = \frac{T_f - T_0}{T_0},$$

$$\beta_T = \frac{hA_s L}{\rho C_p v}, \quad B_T = \frac{-(\Delta H)C_{A0}}{\rho C_p T_0},$$

$$B_C = \frac{k_0 C_{A0} e^{-E/RT_0} L}{v}$$

$$(20)$$

where T_0 and C_0 are the reference temperature and concentration, respectively, to write the system of eqs 18 and 19 in the following form:

$$\frac{\partial \bar{x}_1}{\partial \bar{t}} = -\frac{\partial \bar{x}_1}{\partial \bar{z}} + \frac{1}{Pe_1}\frac{\partial^2 \bar{x}_1}{\partial \bar{z}^2} + B_T B_C \exp\left(\frac{\gamma \bar{x}_1}{1 + \bar{x}_1}\right)(1 + \bar{x}_2)^2$$
$$+ \beta_T(T_s - \bar{x}_1)$$

$$\frac{\partial \bar{x}_2}{\partial \bar{t}} = -\frac{\partial \bar{x}_2}{\partial \bar{z}} + \frac{1}{Pe_2}\frac{\partial^2 \bar{x}_2}{\partial \bar{z}^2} - B_C \exp\left(\frac{\gamma \bar{x}_1}{1 + \bar{x}_1}\right)(1 + \bar{x}_2)^2$$

$$(21)$$

subject to the following boundary conditions:

$$\bar{z} = 0: \quad \frac{\partial \bar{x}_1}{\partial \bar{z}} = Pe_1(\bar{x}_1 - T_i), \quad \frac{\partial \bar{x}_2}{\partial \bar{z}} = Pe_2(\bar{x}_2 - u)$$

$$\bar{z} = 1: \quad \frac{\partial \bar{x}_1}{\partial \bar{z}} = 0, \quad \frac{\partial \bar{x}_2}{\partial \bar{z}} = 0$$

$$(22)$$

Furthermore, in order to simplify the computation of the eigenvalues and eigenfunctions of the spatial differential operator which will be used in our calculations, we insert the non-homogeneous part of the boundary conditions of eq 22 into the differential equation and obtain the following nonlinear parabolic partial differential equation (PDE) model for the process (we suppress the bar notation for $\bar{t}$ and $\bar{z}$):[4]

$$\frac{\partial \bar{x}_1}{\partial t} = -\frac{\partial \bar{x}_1}{\partial z} + \frac{1}{Pe_1}\frac{\partial^2 \bar{x}_1}{\partial z^2} + \delta(z - 0)T_i + B_T B_C$$
$$\exp\left(\frac{\gamma \bar{x}_1}{1 + \bar{x}_1}\right)(1 + \bar{x}_2)^2 + \beta_T(T_s - \bar{x}_1)$$

$$\frac{\partial \bar{x}_2}{\partial t} = -\frac{\partial \bar{x}_2}{\partial z} + \frac{1}{Pe_2}\frac{\partial^2 \bar{x}_2}{\partial z^2} + \delta(z - 0)u - B_C$$
$$\exp\left(\frac{\gamma \bar{x}_1}{1 + \bar{x}_1}\right)(1 + \bar{x}_2)^2$$

$$(23)$$

where δ is the standard Dirac function, subject to the following transformed boundary conditions:

$$z = 0: \quad \frac{\partial x_1}{\partial z} = Pe_1 x_1, \quad \frac{\partial x_2}{\partial z} = Pe_2 x_2$$

$$z = 1: \quad \frac{\partial x_1}{\partial z} = 0, \quad \frac{\partial x_2}{\partial z} = 0$$

$$(24)$$

Finally, we present the solution to the eigenvalue problem of the spatial differential operator of the process, i.e.,

$$-\frac{d\phi_{ij}}{dz} + \frac{1}{Pe_i}\frac{d^2\phi_{ij}}{dz^2} = \lambda_{ij}\phi_{ij}$$

$$(25)$$

subject to

$$z = 0: \quad \frac{d\phi_{ij}}{dz} = Pe_i \phi_{ij}$$

$$z = 1: \quad \frac{d\phi_{ij}}{dz} = 0$$

$$(26)$$

for $i = 1, 2, j = 1, ..., \infty$. The index i is used to denote the ith PDE, and the index j is used to denote the jth eigenmode. The solution of the eigenvalue problem of the spatial differential operator of the ith PDE can be obtained by utilizing standard techniques from linear operator theory and is of the form

$$\lambda_{ij} = -\frac{\bar{a}_{ij}^2}{Pe_i} - \frac{Pe_i}{4}$$

$$\phi_{ij}(z) = B_{ij} \exp\left(Pe_i \frac{z}{2}\right)\left(\cos(\bar{a}_{ij}z) + \frac{Pe_i}{2\bar{a}_{ij}}\sin(\bar{a}_{ij}z)\right)$$

$$\bar{\phi}_{ij}(z) = \exp(-Pe_i z)\phi_{ij}(z)$$

$$(27)$$

for $i = 1, 2, j = 1, ..., \infty$, where λ_{ij}, ϕ_{ij}, and $\bar{\phi}_{ij}$ denote the eigenvalues, eigenfunctions, and adjoint eigenfunctions of the spatial differential operator of the ith PDE, respectively. The parameters B_{ij} and $\bar{a}_{ij}$ can be calculated from the following formulas:

$$B_{ij} = \left[\int_0^1 \left(\cos(\bar{a}_{ij}z) + \frac{Pe_i}{2\bar{a}_{ij}}\sin(\bar{a}_{ij}z)\right)^2 dz\right]^{-1/2}$$

$$\tan \bar{a}_{ij} = \frac{Pe_i \bar{a}_{ij}}{\bar{a}_{ij}^2 - (Pe_i/2)^2}$$

$$(28)$$

for $i = 1, 2, j = 1, ..., \infty$.

The following typical values are given to the process parameters: $Pe_1 = 7$, $Pe_2 = 7$, $B_T = 2.5$, $B_C = 0.1$, $\beta_T = 2$, $T_s = 0$,

$T_f = 0$, and $\gamma = 10$. In all simulations reported below, the second-order finite-difference method was used to discretize, in space, the two parabolic PDEs describing the tubular reactor and obtain a 400th-order set of ODEs in time describing the tubular reactor behavior; this discretized model was used to describe the process dynamics in all simulations. We note that further increase on the order of the process model led to identical open-loop and closed-loop simulation results.

Remark 6. The Péclet numbers (Pe_1 and Pe_2) essentially quantify the ratio of convective transport phenomena to diffusive transport phenomena. If these numbers are large, convective transport phenomena dominate over the diffusive transport phenomena. If they are small, diffusive transport phenomena dominate over the convective transport phenomena. For processes with $Pe_1 = Pe_2 = c$, where c is a constant on the order of 1, both transport mechanisms are significant and the diffusive and convective phenomena are comparable in importance for both the mass and heat transport. In this work, we are considering processes where both the diffusive and convective phenomena play an important role like in most industrially important transport-reaction processes. The choice of $Pe_1 = Pe_2 = 7$ reflects this point: mass and heat transport are fully coupled (i.e., no time scale separation where the assumption can be made that one of the two equations is at steady state), and both the diffusive and convective phenomena have to be accounted for.

However, this choice of Péclet numbers is not a limitation of our approach, as we can still construct a model on the basis of separation of time scales in the modal space. As pointed out below, the first four eigenvalues (for each PDE) of the spatial differential operator are $\lambda_{11} = \lambda_{21} = -2.36$, $\lambda_{12} = \lambda_{22} = -4.60$, $\lambda_{13} = \lambda_{23} = -9.14$, and $\lambda_{14} = \lambda_{24} = -16.29$. From this analysis, we observe a separation in magnitudes of the first two eigenvalues from the second two eigenvalues. Following our previous work (e.g., ref 12), the error associated with the reduced-order model constructed with the first two eigenvalues will have error on the order of $\varepsilon = |\lambda_1|/|\lambda_3| = O(0.1)$. Please see the "Case 3: High-Order Economic Model Predictive Control Formulation with Both State and Input Constraints" subsection which contains a closed-loop simulation with $Pe_1 = 1$ and $Pe_2 = 7$.

Galerkin's Method. To simplify the presentation of the results, we will work with the amplitudes of the eigenmodes of the PDE. To reduce the PDE model of eq 23 into an ODE model, we take advantage of the orthogonality property of the eigenfunctions. Specifically, using Galerkin's method, we first derive a high-order ODE system for each of the PDEs that describes the temporal evolution of the amplitudes corresponding to the first l_i eigenmodes. The state $\bar{x}_i(z, t)$ for $i = 1, 2$ can be written as the sum of the amplitudes and eigenfunctions of the first l_i eigenmodes:

$$\bar{x}_i(z, t) = \sum_{j=1}^{l_i} a_{ij}(t) \phi_{ij}(z) \tag{29}$$

where $a_{ij}(t)$ and $\phi_{ij}(z)$ are the amplitude and eigenfunction associated with the jth eigenvalue of the spatial differential operator of the ith PDE. Substituting the right-hand side of eq 29 into the ith PDE and taking the inner product of the resulting system with the adjoint eigenfunction, we can construct the temporal evolution of the amplitudes of the ith PDE:

$$\dot{a}_{s,i}(t) = A_{s,i} a_{s,i}(t) + F_{s,i}(a_s(t), a_f(t)) + B_{s,i} u(t), \quad i = 1, 2$$

$$\dot{a}_{f,i}(t) = A_{f,i} a_{f,i}(t) + F_{f,i}(a_s(t), a_f(t)) \quad i = 1, 2 \\ + B_{f,i} u(t), \tag{30}$$

where $a_{s,i}(t) = [a_{s,i1}(t)\ a_{s,i2}(t)\ ...\ a_{s,ij}(t)\ ...\ a_{s,im_i}]'$ with elements $a_{s,ij}(t) \in \text{IR}$ associated with the amplitudes of the first m_i eigenmodes and $a_{f,i}$ is a vector of similar structure to $a_{s,i}(t)$ and is associated with the next $m_i + 1$ to l_i eigenmodes. The notation $a_s(t)$, $a_f(t)$, and $a(t)$ is used to denote the following vectors:

$$a_s(t) = \begin{bmatrix} a_{s,1}(t) \\ a_{s,2}(t) \end{bmatrix}, \quad a_f(t) = \begin{bmatrix} a_{f,1}(t) \\ a_{f,2}(t) \end{bmatrix}, \quad a(t) = \begin{bmatrix} a_s(t) \\ a_f(t) \end{bmatrix} \tag{31}$$

The matrix $A_{s,i} = \text{diag}\{\lambda_{ij}\}$ is an $m_i \times m_i$ matrix (i.e, $j = 1, ..., m_i$), the matrix $A_{f,i} = \text{diag}\{\lambda_{ij}\}$ is an $(l_i - m_i) \times (l_i - m_i)$ matrix (i.e., $j = m_i + 1, ..., l_i$), and the matrices $B_{s,i}$ and $B_{f,i}$ and the nonlinear vector fields $F_{s,i}$ and $F_{f,i}$ can be constructed through the appropriate inner product, e.g.,

$$B_{s,i} = \begin{bmatrix} (\bar{\phi}_{i1}(z), \delta(z - 0)) \\ (\bar{\phi}_{i2}(z), \delta(z - 0)) \\ \vdots \\ (\bar{\phi}_{im_i}(z), \delta(z - 0)) \end{bmatrix} \tag{32}$$

The initial conditions of the ODEs in eq 30 are

$$a_{s,i}(0) = \begin{bmatrix} (\bar{\phi}_{i1}(z), \bar{x}(z, 0)) \\ (\bar{\phi}_{i2}(z), \bar{x}(z, 0)) \\ \vdots \\ (\bar{\phi}_{im_i}(z), \bar{x}(z, 0)) \end{bmatrix},$$

$$a_{f,i} = (0) \begin{bmatrix} (\bar{\phi}_{i(m_i+1)}(z), \bar{x}(z, 0)) \\ (\bar{\phi}_{i(m_i+2)}(z), \bar{x}(z, 0)) \\ \vdots \\ (\bar{\phi}_{il_i}(z), \bar{x}(z, 0)) \end{bmatrix} \tag{33}$$

After truncating the fast subsystem of eq 30, we can construct a low-order finite-dimensional model for the first $j = 1, ..., m_i$ eigenmodes of each PDE:

$$\dot{a}_{s,i}(t) = A_{s,i} a_{s,i}(t) + F_{s,i}(a_s(t), 0) + B_{s,i} u(t), \quad i = 1, 2 \tag{34}$$

with initial conditions constructed using a similar procedure as in eq 33. Using eq 27, the first four eigenvalues of the spatial operator of the ith PDE are $\lambda_{11} = \lambda_{21} = -2.36$, $\lambda_{12} = \lambda_{22} = -4.60$, $\lambda_{13} = \lambda_{23} = -9.14$, and $\lambda_{14} = \lambda_{24} = -16.29$. These values indicate that the eigenspectrum exhibits a two-time-scale property. Therefore, we consider the first two eigenvalues, namely, $m_1 = m_2 = 2$, as the dominant/slow eigenmodes and the remaining infinite eigenmodes as the fast ones. We will refer to the ODE system of eq 34 with $m_1 = m_2 = 2$ as the low-order model.

We can also account for the fast subsystem by retaining the first l_i eigenmodes of each PDE. As described previously in the "High-Order Economic Model Predictive Control Formulation"

subsection, the nonlinear part of the fast subsystem can be neglected to improve the computational efficiency. The resulting ODE system is given by

$$\dot{a}_{s,i}(t) = A_{s,i}a_{s,i}(t) + F_{s,i}(a_s(t), a_f(t)) + B_{s,i}u(t), \quad i = 1, 2$$

$$\dot{a}_{f,i}(t) = A_{f,i}a_{f,i}(t) + B_{f,i}u(t), \qquad\qquad i = 1, 2 \tag{35}$$

To determine the amount of eigenmodes to retain, a series of open-loop and closed-loop simulations were preformed. On the basis of these simulation results, the same open-loop and closed-loop results are obtained with a 400th-order discretization, obtained by Galerkin's method ($m_1 = m_2 = 2$ and $l_1 = l_2 = 200$), of the two parabolic PDEs as with the 400th order set of ODEs obtained through the second-order finite-difference method. We will refer to the ODE system of eq 35 with $m_1 = m_2 = 2$ and $l_1 = l_2 = 200$ simply as the high-order model.

Remark 7. In this example, the same number of eigenmodes for each of the two PDEs is retained. However, this is not necessary, in general, hence, the need for the index i.

Implementation of EMPC to a Tubular Reactor. We now proceed with the description and implementation of the EMPC formulations. To solve the EMPC optimization problem at each sampling period, the open-source interior point solver Ipopt[31] was used. To numerically integrate the finite-dimensional ODE model of the transport-reaction process, the explicit Euler method was used with an interation step of 10^{-5}. For the EMPC formulations, we consider a quadratic Lyapunov function of form

$$V(a) = a'(t)Pa(t) \tag{36}$$

where P is an $(m_1 + m_2)$ by $(m_1 + m_2)$ and $(l_1 + l_2)$ by $(l_1 + l_2)$ identity matrix for the low-order and high-order model, respectively, and $\bar{\rho} = 3$ which has been chosen through closed-loop simulations of the PDE system of eq 23 with the low-order EMPC formulated below as an estimate of the closed-loop stability region. The control objective that we consider is to maximize the total reaction rate along the length of the reactor and over one process operation period for $t_f = 1$. The economic measure used to accomplish this objective is

$$L(x, u) = \int_0^1 r(z, t)\, dz \tag{37}$$

where $r(z, t) = k_0 \exp(-E/RT)C_A^2$ is the reaction rate in the tubular reactor.

The control input is subject to constraint as follows: $-1 \leq u \leq 1$. We also consider that there is limitation on the amount of reactant material which can be used over one period t_f. Specifically, the control input trajectory of u should satisfy the following constraint:

$$\frac{1}{t_f}\int_0^{t_f} u(\tau)\, d\tau = 0.5 \tag{38}$$

This constraint means that the total amount of reactant during one period is fixed. We will refer to eq 38 as the reactant material constraint or the integral input constraint. Since the EMPC is evaluated at discrete-time instants during the closed-loop simulation, the reactant material constraint is enforced as follows:

$$\sum_{i=0}^{M-1} u(t_i) = \frac{t_f}{2\Delta} \tag{39}$$

where $M = t_f/\Delta$. Moreover, to ensure that the reactant material constraint is satisfied through the period t_f, the EMPC utilizes the previously computed input $u(t_i)$, $i = 0, 1, ..., (k-1)$ to constrain the control input trajectory $u(t)$, $t \in [t_k, t_{k+N})$, at the current sampling time t_k:

$$\frac{M}{2} + \left(M - \frac{t_k}{\Delta} - N\right)u_{\min} \leq \sum_{i=0}^{k-1} u^*(t_i) + \sum_{j=k}^{N+k} u(t_j)$$

$$\leq \frac{M}{2} + \left(M - \frac{t_k}{\Delta} - N\right)u_{\max} \tag{40}$$

where $M/2$ is the total amount of material that can be supplied to the reactor over one operating period, M is the total number of sampling periods over each operating period, and t_k/Δ is the number of sampling periods since the beginning of the operating period. To simplify the notation, we use the notation $u \in g(t_k)$ to denote this constraint.

In terms of the state constraint, we consider that the temperature T along the length of the reactor is subject to the following constraint:

$$x_{1,\min} \leq x_1(z, t) \leq x_{1,\max} \tag{41}$$

where $x_{1,\min} = -1$ and $x_{1,\max} = 3$ are the lower and upper limits, respectively. Since the models used in the formulations of the EMPC optimization problems are the low-order and high-order models, we cast the state constraint in terms of the amplitudes of the eigenmodes to prevent unnecessary computation required to convert from the modal space back to the state space when solving the optimization problem at each sampling period:

$$-1 \leq \sum_{j=1}^{200} a_{1j}(t)\phi_{1j}(z) \leq 3 \tag{42}$$

Remark 8. The operating period t_f is chosen to be on the order of the time scale of the process dynamics and is used for imposing the integral input constraint (i.e., the available amount of reactant material over one operating period is fixed). Since the reaction is second-order, the optimal strategy to maximize the reaction rate (without the integral constraint) would be to feed the maximum allowable amount of reactant material to the reactor for all time. From a practical (economic) perspective, it is more important to address the case where the available reactant material is fixed. For this case, the EMPC determines the optimal distribution method of the reactant material to the reactor to maximize the reaction rate. As the results of the first simulation case (input constraint only) demonstrate, for a fixed amount of reactant material over some finite-time operating window, it is better, from an economic standpoint, to distribute the material in a periodic fashion, as this distribution method yields greater average production rates over each operation period compared to uniform in time distribution of the reactant material to the reactor.

We also note that the input and integral constraints are imposed for two fundamentally different reasons. The input constraint is imposed as a result of the physical limitations of the control actuator or available control actuation (e.g., the limits on available actuation with a flow valve are fully closed or fully open). As pointed out above, the integral material constraint is an economic or practical constraint that the EMPC must satisfy. For example, consider the case where the integral constraint and input constraint are imposed on the EMPC (no state constraint). If the integral constraint was imposed, but not the input

constraints, the EMPC would choose to feed in all the material over the first sampling period to maximize the reaction rate which is not practical and most likely not physically possible due to control actuator limitations. If we imposed the input constraint, but not the integral constraint, the EMPC would feed in the maximum allowable material for all time which is not as practical as considering the best method to distribute a fixed amount of reactant material to the reactor over time. Therefore, the input and integral constraints taken together are not overlapping.

Case 1: Low-Order Economic Model Predictive Control Formulation with Input Constraint. In the first set of simulations, we propose a low-order EMPC formulation using the low-order model of eq 34 and considering only input constraints which takes the following form for the tubular reactor example:

$$\max_{u \in S(\Delta)} \quad \frac{1}{N\Delta} \int_{t_k}^{t_{k+N}} \left(\int_0^1 r(z, \tau) \, dz \right) d\tau \tag{43a}$$

$$\text{s.t.} \quad \dot{a}_{s,i}(t) = A_{s,i} a_{s,i}(t) + F_{s,i}(a_s(t), 0) \\ + B_{s,i} u(t), \quad i = 1, 2 \tag{43b}$$

$$a_{s,ij}(t_k) = (\bar{\phi}_{s,ij}(z), \bar{x}_i(z, t_k)), \tag{43c}$$
$$i = 1, 2, j = 1, 2$$

$$-1 \le u(t) \le 1, \forall \, t \in [t_k, t_{k+N}) \tag{43d}$$

$$u \in g(t_k) \tag{43e}$$

$$a_s'(t) P a_s(t) \le \bar{\rho} \tag{43f}$$

where $g(t_k)$ is the control input constraint to make the computed input profile over the entire operating period, t_f, satisfy the integral reactant material constraint. The economic cost function of eq 43a that the EMPC works to maximize is the average reaction rate along the length of the reactor. The EMPC of eq 43 is implemented with a prediction horizon $N = 3$ and sampling time $\Delta = 0.01$.

For an initial condition $x(z, 0) = 0$, the manipulated input and closed-loop state profiles under the EMPC controller of eq 43 are shown in Figures 2 and 3/4, respectively. It has been pointed out (e.g., refs 32−34) that, by periodic operation through switching between the upper and lower bounds on the reactant material feed concentration, the average production rate can be improved owing to the second-order dependence of the reaction rate on reactant concentration. Thus, to achieve the maximum reaction rate over one operation period, the EMPC feeds the maximum allowable amount of reactant material to the reactor at the beginning of the process operation period. After a while, the EMPC needs to satisfy the reactant material constraint, so it decreases the amount of reactant material fed to the reactor to the lowest allowable amount, as displayed in Figure 2. We also completed a simulation where the reactant material is fed to the reactor uniformly in time and the input profile is given in Figure 2 (dotted black line). The corresponding closed-loop evolution of the state profiles is given in Figures 5 and 6.

In order to confirm that the economic measure from the manipulated input profile under the low-order EMPC formulation is better than that from uniform in time distribution of the reactant material, we compare the reaction rate values along the length of the reactor from these two input distribution profiles in Figure 7. The average reaction rate along the length of the reactor (i.e., $J = (1/L) \int_0^L r(z, t) \, dz$) under the low-order EMPC formulation of eq 43 increases much faster than that from
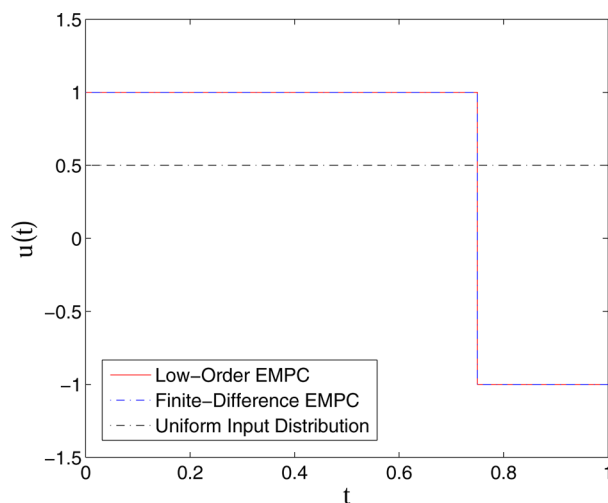

Figure 2. Manipulated input profiles under the EMPC formulation of eq 43 (solid red line), under uniform in time distribution of the reactant material (dotted black line), and under the finite-difference EMPC (dotted blue line) over one operation period. The input profiles of the two EMPCs (solid red line and dotted blue line) are overlapping.
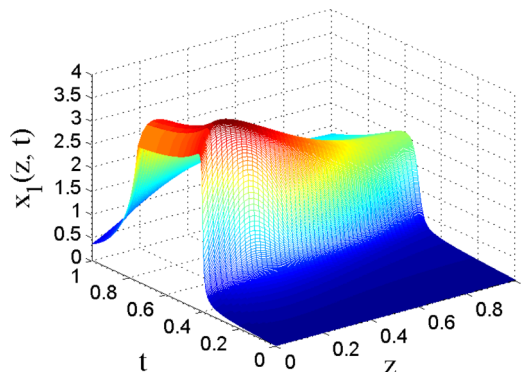

Figure 3. Closed-loop profile of x_1 under the low-order EMPC formulation of eq 43 over one operation period.
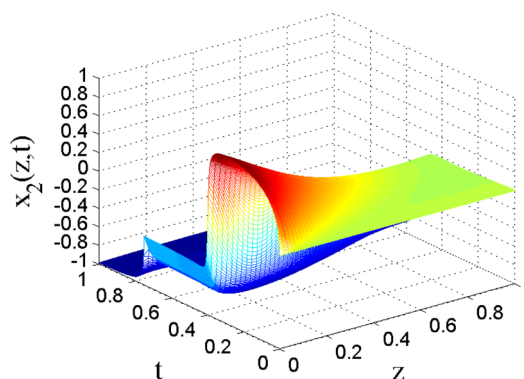

Figure 4. Closed-loop profile of x_2 under the low-order EMPC formulation of eq 43 over one operation period.

uniform in time distribution of the reactant material because of the second-order reaction and the EMPC input distribution. Over this one operation period, the total reaction rate from the system under the EMPC formulation is about 15.45% higher than that from the closed-loop system under flat input distribution.
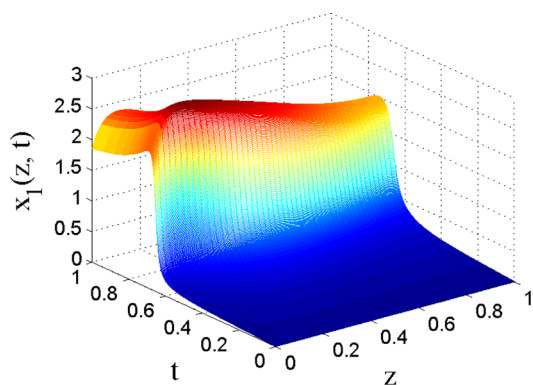
Figure 5. Closed-loop profile of x_1 under uniform in time distribution of the reactant material over one operation period.
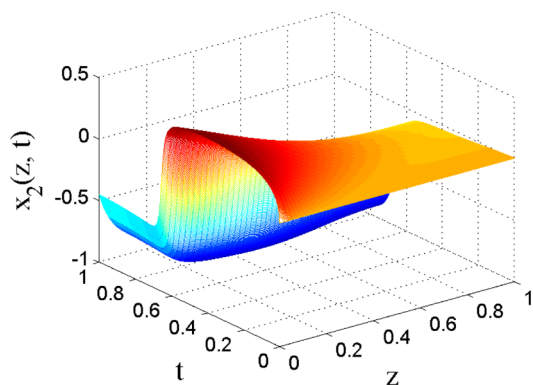

Figure 6. Closed-loop profile of x_2 under uniform in time distribution of the reactant material over one operation period.
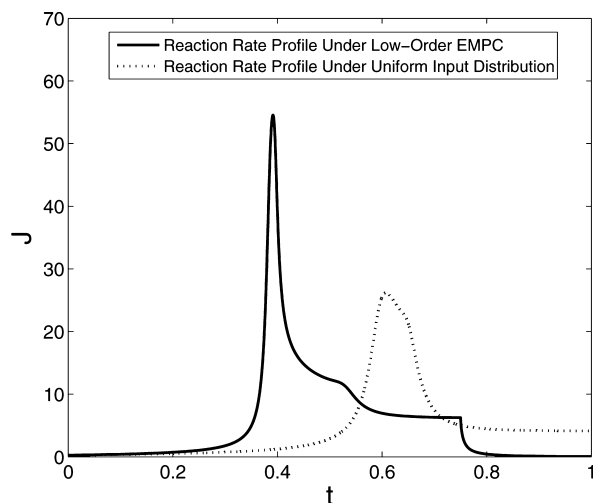

Figure 7. Average reaction rate J along the length of the reactor (i.e., $J = (1/L) \int_0^L r(z, t) \, dz$) under the low-order EMPC formulation of eq 43 over one operation period (solid line) and under uniform in time distribution of the reactant material (dashed line).

To verify the accuracy of the low-order EMPC, we formulate an EMPC with the 400-order finite-difference method, which we refer to as the finite-difference EMPC, to compare the closed-loop evolution obtained under the finite-difference EMPC with the low-order EMPC. The manipulated input profile under the finite-difference method is also shown in Figure 2. From this simulation, the same input profile is computed by the high-order finite-difference EMPC as the low-order EMPC. However, the

low-order model uses four ODEs to predict the future evolution of the PDE system, while the high-order finite-difference EMPC uses 400 ODEs. From Figure 8, we observe a significant
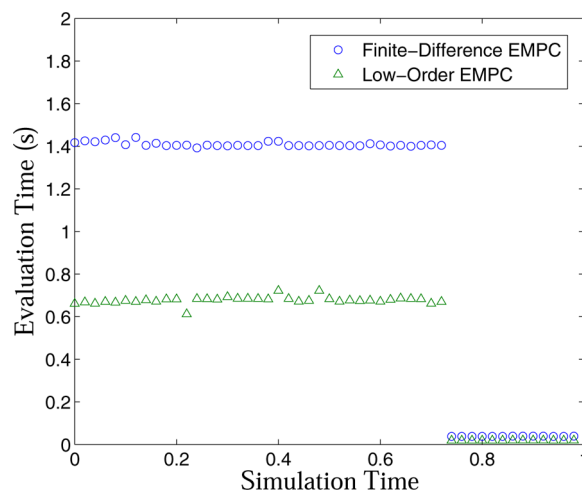
Figure 8. Computational time required to solve the low-order EMPC optimization problem and the finite-difference EMPC optimization problem over one operation period.

computational improvement with using the low-order EMPC. Furthermore, if we formulate an EMPC with a fourth-order model obtained through the finite-difference method and apply it to the PDE system, the resulting EMPC does not compute the optimal trajectory, as it cannot accurately predict the future evolution of the system.

Since chemical reactors are typically operated continuously over long periods of time, we conduct another simulation of multiple (20) consecutive periods of operation. The reactant material constraint is enforced over each of the 20 consecutive operating periods where the system at the beginning of each period starts from a different initial condition. Figure 9 displays
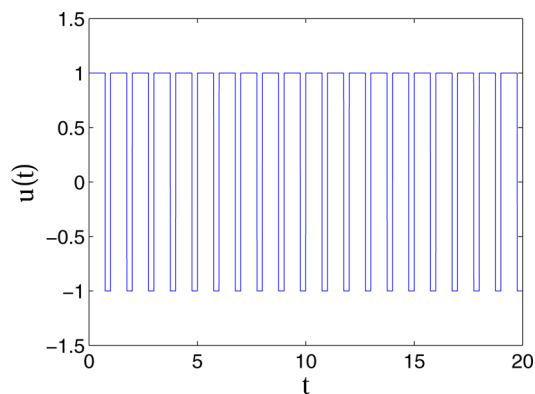

Figure 9. Twenty-period operation manipulated input profile under the low-order EMPC formulation of eq 43.

the manipulated input profiles under the EMPC controller of eq 43, and Figures 10 and 11 depict the closed-loop evolution of the two states under the low-order EMPC formulation of eq 43, respectively. After two operation periods in the 20-period operation simulation under the low-order EMPC of eq 43, the closed-loop economic measure becomes constant over each operation period, as shown in Figure 12. The total reaction rate over each operation period under the low-order EMPC after two
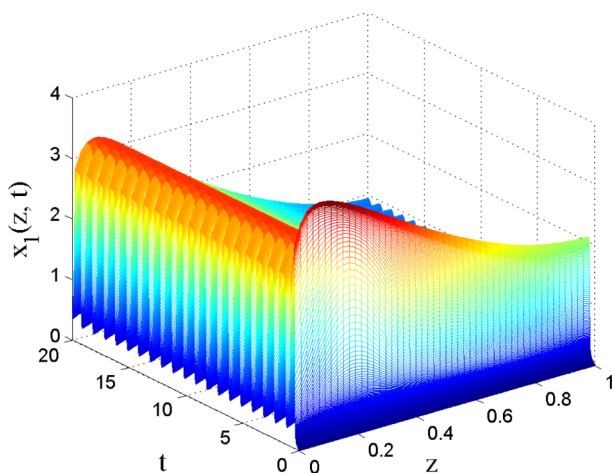
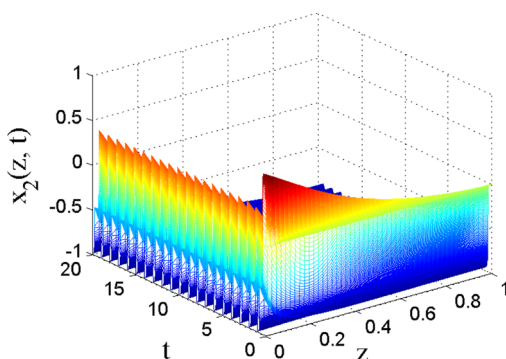**Figure 10.** Twenty-period operation closed-loop profile of x_1 under the low-order EMPC formulation of eq 43.

Figure 11. Twenty-period operation closed-loop profile of x_2 under the low-order EMPC formulation of eq 43.
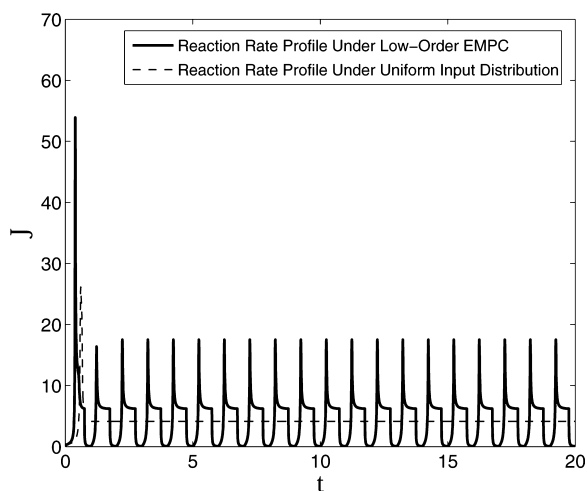

Figure 12. Average reaction rate along the length of the reactor J (i.e., $J = (1/L)\int_0^L r(z, t)\, dz$) under the low-order EMPC formulation of eq 43 over a 20-period operation (solid line) and under uniform in time distribution of the reactant material (dashed line).

operation periods is still 3.89% greater than that of the case under uniform in time distribution of the reactant material.

Remark 9. Regarding the oscillations (e.g., Figures 9–12 where the evolution of the tubular reactor is simulated over 20 operating intervals and the process evolution appears to be oscillatory), we point out that this is not open-loop periodic

behavior or a numerical issue. This behavior is enforced by the EMPC to maximize the cost over many periods. We refer the interested reader to any of the literature on periodically operated reactors (e.g., refs 33 and 34) for more commentary on this issue.

Case 2: High-Order Economic Model Predictive Control Formulation with State and Actuator Constraints. Second, we consider the addition of a state constraint and use the high-order EMPC formulation of eq 17 with the high-order model of eq 35; the average reactant material constraint is removed. The high-order EMPC formulation for this chemical process example has the following form:

$$\max_{u \in S(\Delta)} \quad \frac{1}{N\Delta} \int_{t_k}^{t_{k+N}} \left(\int_0^1 r(z, \tau)\, dz \right) d\tau \tag{44a}$$

$$\text{s.t.} \quad \dot{a}_{s,i}(t) = A_{s,i}a_{s,i}(t) + F_{s,i}(a_s(t),\, a_f(t)) \\ + B_{s,i}u(t), \quad i = 1, 2 \tag{44b}$$

$$\dot{a}_{f,i}(t) = A_{f,i}a_{f,i}(t) + B_{f,i}u(t), \quad i = 1, 2 \tag{44c}$$

$$a_{s,ij}(t_k) = (\bar{\phi}_{s,ij}(z), \bar{x}_i(z, t_k)), \\ i = 1, 2,\, j = 1, 2 \tag{44d}$$

$$a_{f,ij}(t_k) = (\bar{\phi}_{f,ij}(z), \bar{x}_i(z, t_k)), \\ i = 1, 2,\, j = 3, \dots, 200 \tag{44e}$$

$$-1 \leq \sum_{j=1}^{200} a_{1j}(t)\phi_{1j}(z) \leq 3 \tag{44f}$$

$$-1 \leq u(t) \leq 1,\, \forall\, t \in [t_k, t_{k+N}) \tag{44g}$$

$$a'(t)Pa(t) \leq \bar{\rho} \tag{44h}$$

The EMPC of eq 44 is implemented with a prediction horizon $N = 5$ and sampling time $\Delta = 0.02$. The prediction horizon N and sampling time Δ are greater than case 1 to increase the overall prediction horizon length, which helps to guarantee that the temperature does not violate its upper nor lower limit. For this case, the initial condition is the steady state of the system under uniform input distribution, $u = 0.5$, as shown in Figures 5 and 6.

The manipulated input and closed-loop state profiles under the high-order EMPC of eq 44 are shown in Figures 13 and 14/15, respectively. From Figure 13, the EMPC initially feeds in more reactant material to the reactor to increase the reaction rate. Since the reaction is exothermic, the temperature in the reactor also increases. When the temperature approaches the maximum allowable temperature, the input reactant concentration decreases to avoid the temperature in the reactor from exceeding $x_{1,\max} = 3$. After this phase, the high-order EMPC maintains operation at a steady state associated with the maximum temperature in the reactor being equal to the maximum allowable temperature. For this simulation, the corresponding maximum temperature in the reactor trajectory is shown in Figure 16.

We compare the closed-loop evolution of the tubular reactor under the high-order EMPC and under the high-order finite-difference EMPC formulated with the state constraint (no integral input constraint). The manipulated input profile computed by the finite-difference EMPC is shown in Figure 13 (dotted blue line) along with the profile of the high-order EMPC. The closed-loop state trajectories under the finite-difference EMPC are shown in Figures 17 and 18. The overall difference between the two input trajectories is small, as shown in Figure 13,
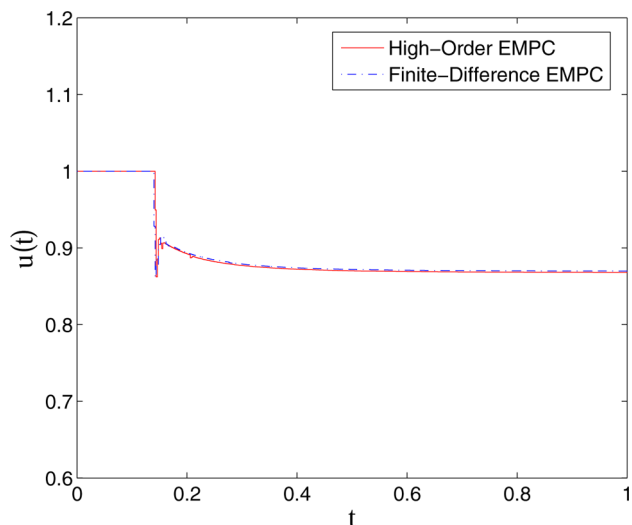
Figure 13. Manipulated input profile under the high-order EMPC formulation of eq 44 (solid red line) and under the finite-difference EMPC (dotted blue line) over one operation period.
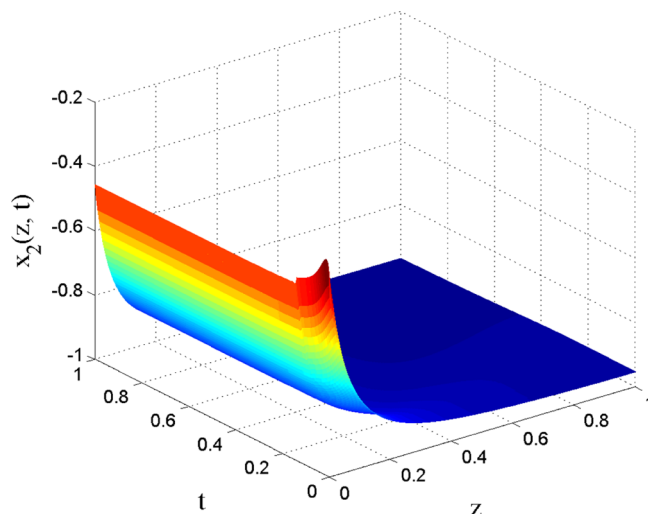

Figure 14. Closed-loop profile of x_1 under the high-order EMPC formulation of eq 44 over one operation period.
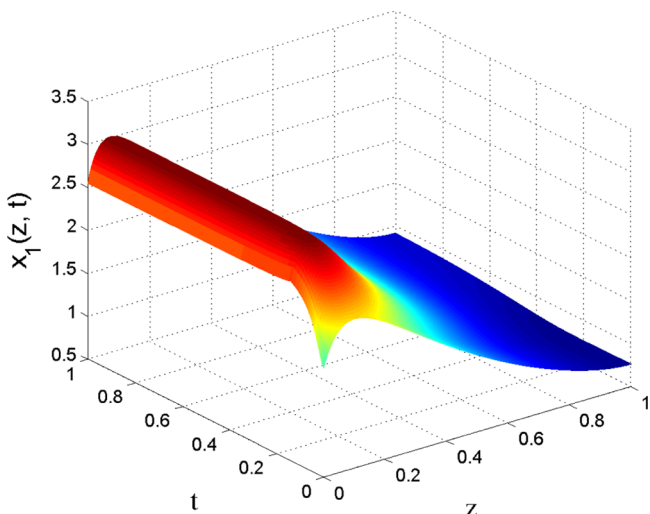

Figure 15. Closed-loop profile of x_2 under the high-order EMPC formulation of eq 44 over one operation period.
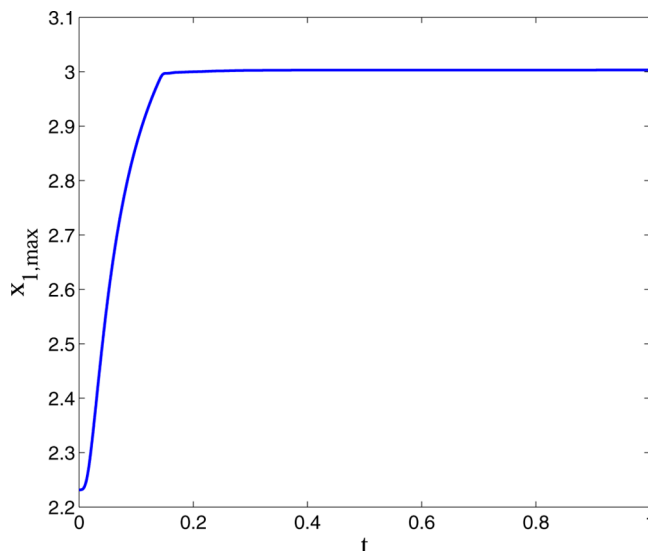

Figure 16. Closed-loop profile of the maximum value of x_1 along the length of the reactor under the high-order EMPC formulation of eq 44 over one operation period.

Figure 17. Closed-loop profile of x_1 under the finite-difference EMPC formulation with the state constraint over one operation period.

and as a result, the closed-loop states under the high-order EMPC and under the finite-difference EMPC evolve in a similar fashion. Since both EMPCs use a 400-order model albeit obtained through different methods, the computational time required to solve the EMPC optimization problems are comparable.

Case 3: High-Order Economic Model Predictive Control Formulation with Both State and Input Constraints. Finally, we add the reactant material constraint into the high-order EMPC formulation, and thus, the high-order EMPC formulation considering both the state and input constraints for this chemical process example has the following form:
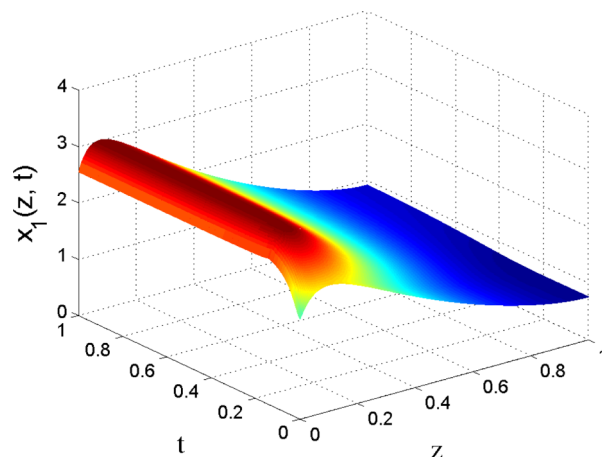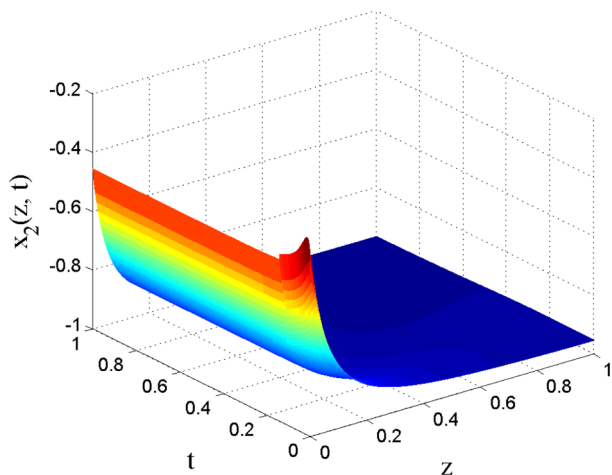
Figure 18. Closed-loop profile of x_2 under the finite-difference EMPC formulation with the state constraint over one operation period.

$$\max_{u \in S(\Delta)} \quad \frac{1}{N\Delta} \int_{t_k}^{t_{k+N}} \left(\int_0^1 r(z, \tau) \, dz \right) d\tau \tag{45a}$$

$$\text{s.t.} \quad \dot{a}_{s,i}(t) = A_{s,i} a_{s,i}(t) + F_{s,i}(a_s(t), a_f) \\ + B_{s,i} u(t), \quad i = 1, 2 \tag{45b}$$

$$\dot{a}_{f,i}(t) = A_{f,i} a_{f,i}(t) + B_{f,i} u(t), \quad i = 1, 2 \tag{45c}$$

$$a_{s,ij}(t_k) = (\bar{\phi}_{s,ij}(z), \bar{x}(z, t_k)), \tag{45d}$$
$$i = 1, 2, j = 1, 2$$

$$a_{f,ij}(t_k) = (\bar{\phi}_{f,ij}(z), \bar{x}_i(z, t_k)), \tag{45e}$$
$$i = 1, 2, j = 3, ..., 200$$

$$-1 \leq \sum_{j=1}^{200} a_{1j}(t) \phi_{1j}(z) \leq 3 \tag{45f}$$

$$-1 \leq u(t) \leq 1, \, \forall \, t \in [t_k, t_{k+N}) \tag{45g}$$

$$u \in g(t_k) \tag{45h}$$

$$a'(t) P a(t) \leq \bar{\rho} \tag{45i}$$

We consider the prediction horizon $N = 5$ and sampling time $\Delta = 0.02$. For this case, the initial condition is the steady state of the system under uniform input distribution, $u = 0.5$, as shown in Figures 5 and 6.

Figures 19 and 20 show the closed-loop evolution of the states under the EMPC formulation of eq 45. The corresponding manipulated input profiles are given in Figure 21 (solid line). Here, again, the EMPC initially feeds in the maximum allowable reactant material until the maximum allowable temperature in the reactor is reached and the EMPC feeds less reactant material to the reactor to maintain operation at the maximum allowable temperature. In the beginning, the optimal input trajectory follows a similar path to case 2, since the input constraint has no effect on the choice of the optimal input value. After some time, the reactant material constraint needs to be satisfied, so the input reactant concentration decreases at $t = 0.8$ to satisfy the constraint. The corresponding highest temperature in the reactor also decreases when the input is limited by the reactant material constraint, as shown in Figure 22.
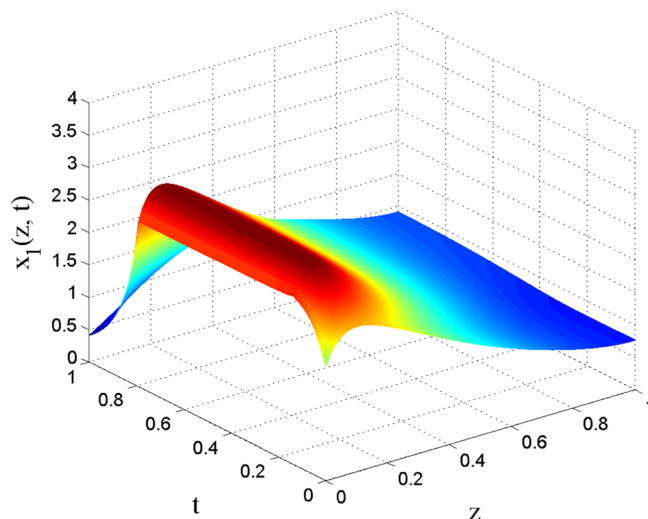

Figure 19. Closed-loop profile of x_1 under the high-order EMPC formulation of eq 45 over one operation period.
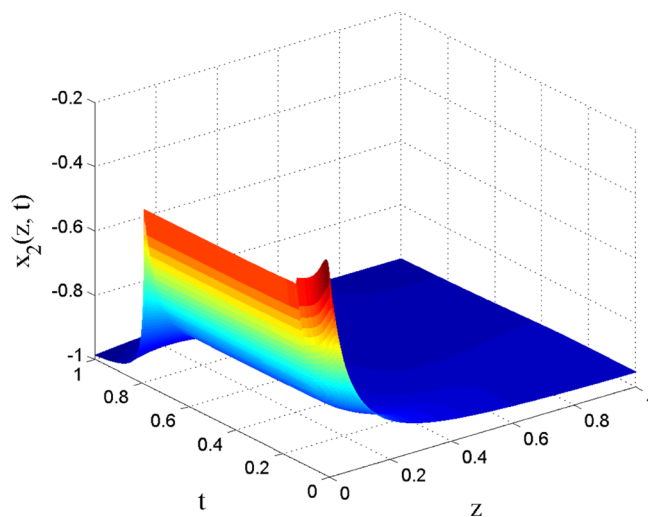

Figure 20. Closed-loop profile of x_2 under the high-order EMPC formulation of eq 45 over one operation period.
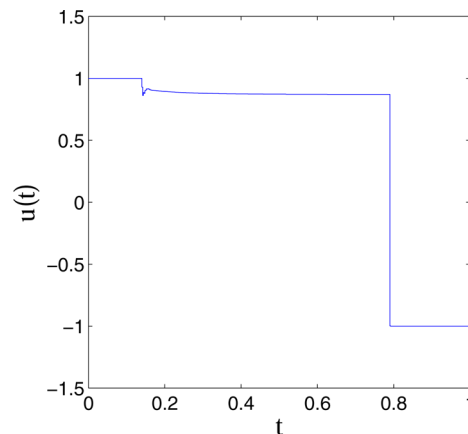

Figure 21. Manipulated input profile under the high-order EMPC formulation of eq 45 over one operation period.

For this case study, in order to confirm that the economic measure from the control input profile under the high-order EMPC formulation is better than that from the system under
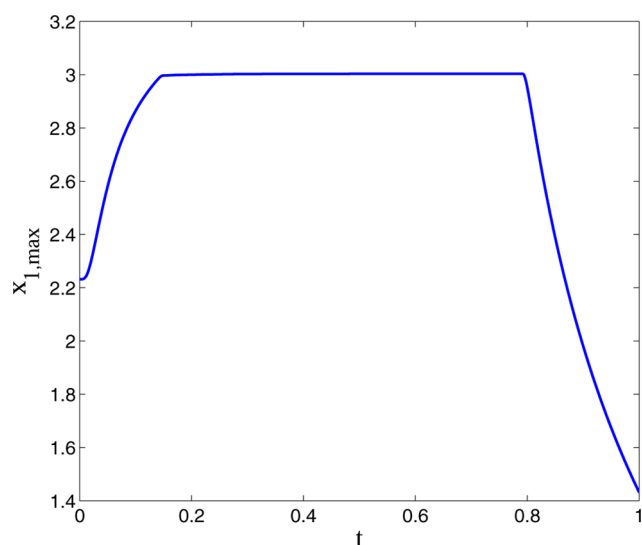
Figure 22. Closed-loop profile of the maximum value of x_1 along the length of the reactor under the high-order EMPC formulation of eq 45 over one operation period.

uniform in time distribution of the reactant material, we compare the reaction rate along the length of the reactor from these two input distribution profiles, shown in Figure 23. Since the initial
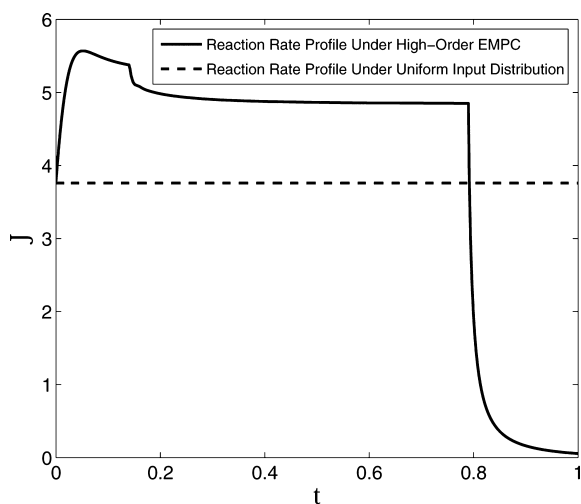

Figure 23. Average reaction rate along the length of the reactor J (i.e., $J = (1/L)\int_0^L r(z, t)\,\mathrm{d}z$) under the high-order EMPC formulation of eq 45 over one operation period (solid line) and under uniform in time distribution of the reactant material (dashed line).

condition for this case study is the steady state of the system under uniform input distribution, the overall reaction rate is a constant throughout the operation period when the reactant material is distributed uniformly in time to the reactor. On the other hand, the average reaction rate along the length of the reactor, J, under the EMPC formulation of eq 45 increases dramatically because of the second-order reaction, and after some time, it reaches a steady state when the input is held constant. Lastly, it drops to zero, since the reactant material constraint needs to be satisfied over one operation period. Over this one operation period, the total reaction rate from the system under the EMPC formulation is still 6.91% higher than that from the system under uniform in time distribution of the reactant material.

To demonstrate that the EMPC performance is not associated with the specific process parameters, we conduct another simulation where $Pe_1 = 1$. This represents the case where the time scales of heat diffusive and convective phenomena are roughly equivalent and the heat convective phenomena are slower than the mass convective phenomena compared to the case where $Pe_1 = 7$. As a result of the slower heat convection, the temperature does not increase as much over the course of the one operating period simulation compared to the case with $Pe_1 = 7$. To demonstrate the ability of the high-order EMPC to satisfy state constraint, we set the maximum allowable temperature to be $x_{1,max} = 2$. The closed-loop state and manipulated input profiles are shown in Figures 24–26, respectively. Over the one
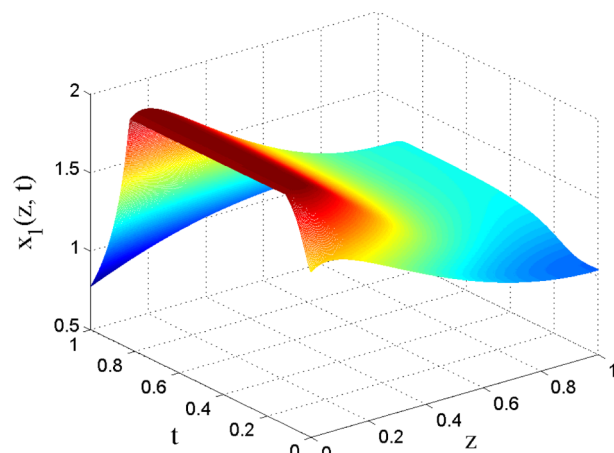

Figure 24. Closed-loop profile of x_1 under the high-order EMPC formulation of eq 45. For this case, the heat transfer Péclet number is $Pe_1 = 1$.
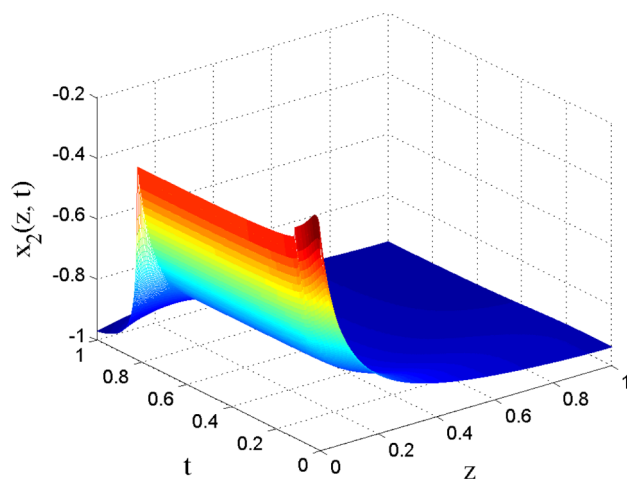

Figure 25. Closed-loop profile of x_2 under the high-order EMPC formulation of eq 45. For this case, the heat transfer Péclet number is $Pe_1 = 1$.

operation period (with $Pe_1 = 1$), the total reaction rate from the system under the high-order EMPC is 7.09%. For the case of $x_{1,max} = 3$ and $Pe_1 = 1$, we have also verified that the EMPC will compute the same input profile as case 1 because the upper bound on the temperature is never reached over the course of one operating period.

Remark 10. While the argument can be made that the optimal operating policy of the first simulation (the EMPC formulated
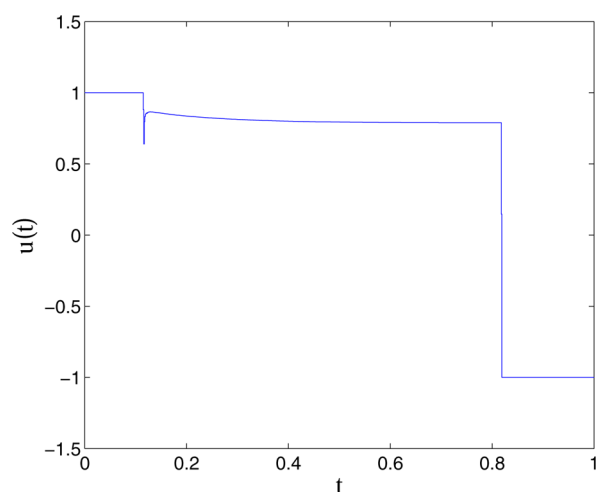
Figure 26. Manipulated input profile under the high-order EMPC formulation of eq 45. For this case, the heat transfer Péclet number is $Pe_1 = 1$.

with an input constraint only) can be determined through physical intuition owing to the second-order reaction rate, our motivation for performing this simulation is to demonstrate that the EMPC, formulated with a low-order model (in this case, the model is constructed with the first four (2×2) modes only), can return the optimal operating strategy. In the subsequent simulation studies, we demonstrate the ability of EMPC to determine a more complex optimal operating strategy in real time while also accounting for other process constraints. Specifically, the EMPC is able to return the optimal operating strategy by considering a state constraint that limits the maximum allowable operating temperature in the reactor.

CONCLUSION

In this work, we developed low-order and high-order finite-dimensional economic model predictive (EMPC) systems, through the application of Galerkin's method and involvement of singular perturbation arguments, for transport-reaction processes described by nonlinear parabolic PDE systems. The formulated EMPC systems were applied to a tubular reactor example described by two nonlinear parabolic PDEs, where the average reaction rate along the length of the reactor was used as the cost function. Closed-loop simulations demonstrated that, in the absence of state constraint, the low-order EMPC system is sufficient to meet the constraint on the availability of the reactant material over one operation period, and yields improved closed-loop economic performance compared to when the reactant material is fed uniformly in time to the reactor by requesting a suitable time-varying reactor operation. On the other hand, when a state constraint on the maximum value of the temperature along the length of the reactor is imposed, the use of a high-order (yet computationally efficient) EMPC system allows one to account for the process dynamics with sufficient accuracy and meet both the input and state constraints simultaneously while improving the economic cost over uniform in time feeding of the reactant material.

AUTHOR INFORMATION

Corresponding Author

*E-mail: pdc@seas.ucla.edu.

Notes

REFERENCES

(1) Smoller, J. *Shock Waves and Reaction-Diffusion Equations*; Grundlehren der mathematischen Wissenschaften; Springer-Verlag: Berlin, Heidelberg, Germany, 1983.

(2) Curtain, R. F.; Pritchard, A. J. *Infinite Dimensional Linear Systems Theory*; Lecture Notes in Control and Information Sciences; Springer-Verlag: Berlin, Heidelberg, Germany, 1978; Vol. 8.

(3) Balas, M. J. Feedback control of linear diffusion processes. *Int. J. Control* **1979**, *29*, 523−534.

(4) Ray, W. H. *Advanced Process Control*; McGraw-Hill: New York, 1981.

(5) Chen, C.-C.; Chang, H.-C. Accelerated disturbance damping of an unknown distributed system by nonlinear feedback. *AIChE J.* **1992**, *38*, 1461−1476.

(6) Temam, R. *Infinite-Dimensonal Dynamical Systems in Mechanics and Physics*; Applied Mathematical Sciences; Springer-Verlag: New York, 1988; Vol. 68.

(7) Foias, C.; Jolly, M. S.; Kevrekidis, I. G.; Sell, G. R.; Titi, E. S. On the computation of inertial manifolds. *Phys. Lett. A* **1988**, *131*, 433−436.

(8) Foias, C.; Sell, G. R.; Titi, E. S. Exponential tracking and approximation of inertial manifolds for dissipative nonlinear equations. *J. Dyn. Differ. Equations* **1989**, *1*, 199−244.

(9) Christofides, P. D.; Daoutidis, P. Finite-dimensional control of parabolic PDE systems using approximate inertial manifolds. *J. Math. Anal. Appl.* **1997**, *216*, 398−420.

(10) Baker, J.; Christofides, P. D. Finite-dimensional approximation and control of non-linear parabolic PDE systems. *Int. J. Control* **2000**, *73*, 439−456.

(11) El-Farra, N. H.; Armaou, A.; Christofides, P. D. Analysis and control of parabolic PDE systems with input constraints. *Automatica* **2003**, *39*, 715−725.

(12) Christofides, P. D. *Nonlinear and Robust Control of PDE Systems: Methods and Applications to Transport-Reaction Processes*; Birkhäuser: Boston, MA, 2001.

(13) García, C. E.; Prett, D. M.; Morari, M. Model predictive control: Theory and practice—A survey. *Automatica* **1989**, *25*, 335−348.

(14) Mayne, D. Q.; Rawlings, J. B.; Rao, C. V.; Scokaert, P. O. M. Constrained model predictive control: Stability and optimality. *Automatica* **2000**, *36*, 789−814.

(15) Rawlings, J. B. Tutorial overview of model predictive control. *IEEE Control Syst. Mag.* **2000**, *20*, 38−52.

(16) Ito, K.; Kunisch, K. Receding horizon optimal control for infinite dimensional systems. *ESAIM: Control, Optim. Calculus Var.* **2002**, *8*, 741−760.

(17) Dufour, P.; Touré, Y.; Blanc, D.; Laurent, P. On nonlinear distributed parameter model predictive control strategy: On-line calculation time reduction and application to an experimental drying process. *Comput. Chem. Eng.* **2003**, *27*, 1533−1542.

(18) Dubljevic, S. Boundary model predictive control of Kuramoto−Sivashinsky equation with input and state constraints. *Comput. Chem. Eng.* **2010**, *34*, 1655−1661.

(19) Dufour, P.; Touré, Y. Multivariable model predictive control of a catalytic reverse flow reactor. *Comput. Chem. Eng.* **2004**, *28*, 2259−2270.

(20) Dubljevic, S.; Mhaskar, P.; El-Farra, N. H.; Christofides, P. D. Predictive control of transport-reaction processes. *Comput. Chem. Eng.* **2005**, *29*, 2335−2345.

(21) Dubljevic, S.; El-Farra, N. H.; Mhaskar, P.; Christofides, P. D. Predictive control of parabolic PDEs with state and control constraints. *Int. J. Robust Nonlinear Control* **2006**, *16*, 749−772.

(22) Dubljevic, S.; Christofides, P. D. Predictive control of parabolic PDEs with boundary control actuation. *Chem. Eng. Sci.* **2006**, *61*, 6239−6248.

(23) Diehl, M.; Amrit, R.; Rawlings, J. B. A Lyapunov function for economic optimizing model predictive control. *IEEE Trans. Autom. Control* **2011**, *56*, 703−707.

(24) Heidarinejad, M.; Liu, J.; Christofides, P. D. Economic model predictive control of nonlinear process systems using Lyapunov techniques. *AIChE J.* **2012**, *58*, 855−870.

(25) Chen, X.; Heidarinejad, M.; Liu, J.; Christofides, P. D. Distributed economic MPC: Application to a nonlinear chemical process network. *J. Process Control* **2012**, *22*, 689−699.

(26) Heidarinejad, M.; Liu, J.; Christofides, P. D. Algorithms for improved fixed-time performance of Lyapunov-based economic model predictive control of nonlinear systems. *J. Process Control* **2013**, *23*, 404−414.

(27) Heidarinejad, M.; Liu, J.; Christofides, P. D. Economic model predictive control of switched nonlinear systems. *Syst. Control Lett.* **2013**, *62*, 77−84.

(28) Holmes, P.; Lumley, J. L.; Berkooz, G. *Turbulence, Coherent Structures, Dynamical Systems and Symmetry*; Cambridge University Press: New York, 1996.

(29) Mhaskar, P.; El-Farra, N. H.; Christofides, P. D. Stabilization of nonlinear systems with state and control constraints using Lyapunov-based predictive control. *Syst. Control Lett.* **2006**, *55*, 650−659.

(30) Scokaert, P. O. M.; Rawlings, J. B. Feasibility issues in linear model predictive control. *AIChE J.* **1999**, *45*, 1649−1659.

(31) Wächter, A.; Biegler, L. T. On the implementation of an interior-point filter line-search algorithm for large-scale nonlinear programming. *Math. Program.* **2006**, *106*, 25−57.

(32) Rawlings, J. B.; Amrit, R. Optimizing process economic performance using model predictive control. In *Nonlinear Model Predictive Control*; Magni, L., Raimondo, D. M., Allgöwer, F., Eds.; Lecture Notes in Control and Information Sciences; Springer: Berlin, Heidelberg, Germany, 2009; Vol. *384*, pp 119−138.

(33) Budman, H.; Silveston, P. L. Control of periodically operated reactors. *Chem. Eng. Sci.* **2008**, *63*, 4942−4954.

(34) Silveston, P. L., Hudgins, R. R., Eds. *Periodic Operation of Reactors*; Elsevier: Oxford, England, 2013.